SCIENCE CHINA
Earth Sciences

SPECIAL TOPIC: Origin of granites and associated mineralization
• RESEARCH PAPER •

July 2017 Vol.60 No.7: 1256–1267
doi: 10.1007/s11430-016-9033-5

Crustal accretion and reworking processes of micro-continental massifs within orogenic belt: A case study of the Erguna Massif, NE China

SUN ChenYang, TANG Jie*, XU WenLiang, LI Yu & ZHAO Shuo

College of Earth Sciences, Jilin University, Changchun 130061, China

Received November 28, 2016; accepted March 20, 2017; published online March 30, 2017

Abstract This paper summarizes the geochronological, geochemical and zircon Hf isotopic data for Mesozoic granitoids within the Erguna Massif, NE China, and discusses the spatial-temporal variation of zircon Hf isotopic compositions, with the aim of constraining the accretion and reworking processes of continental crust within the Erguna Massif, and shedding light on the crustal evolution of the eastern segment of the Central Asian Orogenic Belt. Based on the zircon U-Pb dating results, the Mesozoic granitic magmatisms within the Erguna Massif can be subdivided into five stages: Early-Middle Triassic (249–237 Ma), Late Triassic (229–201 Ma), Early-Middle Jurassic (199–171 Ma), Late Jurassic (155–149 Ma), and Early Cretaceous (145–125 Ma). The Triassic to Early-Middle Jurassic granitoids are mainly I-type granites and minor adakitic rocks, whereas the Late Jurassic to Early Cretaceous granitoids are mainly A-type granites. This change in magmatism is consistent with the southward subduction of the Mongol-Okhotsk oceanic plate and subsequent collision and crustal thickening, followed by post-collision extension. Zircon Hf isotopic data indicate that crustal accretion of the Erguna Massif occurred in the Mesoproterozoic and Neoproterozoic. Zircon $\varepsilon_{\mathrm{Hf}}(t)$ values increase gradually over time, whereas two-stage model (T_{DM2}) ages decrease throughout the Mesozoic. The latter result indicates a change in the source of granitic magmas from the melting of ancient crust to more juvenile crust. Zircon $\varepsilon_{\mathrm{Hf}}(t)$ values also exhibit spatial variations, with values decreasing northwards, whereas T_{DM2} ages increase. This pattern suggests that, moving from south to north, there is an increasing component of ancient crustal material within the lower continental crust of the Erguna Massif. Even if at the same latitude, the zircon Hf isotopic compositions are also inconsistent. These results reveal lateral and vertical heterogeneities in the lower continental crust of the Erguna Massif during the Mesozoic, which we use as the basis of a structural and tectonic model for this region.

Keywords Orogenic belt, The Erguna Massif, Crustal accretion and reworking, Mesozoic, Granitoids, Hf isotope

Citation: Sun C Y, Tang J, Xu W L, Li Y, Zhao S. 2017. Crustal accretion and reworking processes of micro-continental massifs within orogenic belt: A case study of the Erguna Massif, NE China. Science China Earth Sciences, 60: 1256–1267, doi: 10.1007/s11430-016-9033-5

1. Introduction

Unlike the other terrestrial planets, the Earth has a chemically evolved crust, i.e., the felsic continental crust (Campbell and Taylor, 1983; Rudnick, 1995; Jahn et al., 2000a, 2000b, 2000c). Questions about the structure, composition, accretion, and reworking of the continental crust are at the forefront of modern Earth Science research. Continents can be subdivided into two major tectonic units: cratons and orogenic belts. Although there is a large body of research on continental cratons, and it has been widely accepted that the continental cratons formed mainly during the Archean (Taylor and Mclennan, 1985; Jacobsen, 1988; DePaolo et al., 1991; Hawkesworth and Kemp, 2006; Belousova et al., 2010; Dhuime et al., 2011, 2012), less attention has been devoted to understand the evolution of orogenic belts. In particular,

* Corresponding author (email: 893335234@qq.com)

the crustal accretion and reworking processes of micro-continental massifs within orogenic belt are poorly known. Some researches have shown that the crustal accretion within the Central Asian Orogenic Belt (CAOB) mainly took place during the Neoproterozoic and Phanerozoic, which is worthy to make further studies and tests (Wu et al., 2000, 2003; Jahn et al., 2000a, 2000b, 2000c, 2004; Liu et al., 2005; Windley et al., 2007; Guo et al., 2010).

The CAOB is a typical example of an accretionary orogenic belt (Windley et al., 1990, 2007; Jahn et al., 2000a, 2000b, 2000c; Yakubchuk, 2002, 2004; Xiao et al., 2003, 2004), which makes it a good region in which to study the mechanisms of accretion and reworking of the continental crust. The eastern segment of the CAOB passes through NE China, where it comprises a series of micro-continental massifs and orogenic belts, and contains numerous granitic intrusions. These granitoids are the tracers to reveal the accretion and reworking processes of the continental crust (DePaolo et al., 1991; Rudnick, 1995; Wu et al., 2011). Recent geochemical studies of granitoids in NE China have indicated that crustal accretion in this region occurred mainly in the Phanerozoic (Wu et al., 1999, 2011). However, additional evidence suggests that this phase of accretion mainly affected the Paleozoic orogenic belt, and not the micro-continental massifs (Wang et al., 2015; Tang et al., 2015). The mechanisms and accretion and reworking processes of micro-continental massifs within the CAOB are unclear. Therefore, we report geochemical and zircon Hf isotopic data for Mesozoic granitoids within the Erguna Massif in order to resolve these questions, and help constrain the tectonic history of the massifs in NE China. Our observations provide an insight into the processes that affect micro-continental massifs within orogenic belt, and are important for studies of the development of the continental crust elsewhere.

2. Geological background

The Paleozoic tectonic evolution of NE China was dominated by the closure of the Paleo-Asian ocean and the amalgamation of micro-continental massifs (including, from west to east, the Erguna, Xing'an, Songnen-Zhangguangcai Range, Jiamusi and Khanka massifs) (Figure 1a) (Li et al., 1999; Wu et al., 2002, 2007, 2011; Li, 2006; Xu et al., 2009; Meng et al., 2010; Wang F et al., 2012a, 2012b; Cao et al., 2013; Li et al., 2014), whereas the Mesozoic tectonic evolution of NE China was characterized by the overprinting of the circum-Pacific and Mongol-Okhotsk tectonic regimes (Ge et al., 2001; Meng et al., 2011; Yu et al., 2012; Xu W L et al., 2013; Xu M J et al., 2013; Sun D Y et al., 2013; Dong et al., 2014; Tang et al., 2014).

The Erguna Massif is bounded by the Mongol-Okhotsk suture belt to the northwest and by the Xiguitu-Tayuan Fault to the southeast (Figure 1a). Proterozoic, Paleozoic, and Mesozoic strata crop out in this study area. The Proterozoic strata comprise the Xinghuadukou Group, a suite of metamorphosed volcanic and sedimentary rocks, including granitic gneiss, and both basic and acid volcanics; the Jiageda Formation, which includes schist, leptite, and quartzite; and the Ergunahe Formation, which is composed of marble, granulite, leptite, mica-quartz schist, silty slate, crystalline limestone, and meta-arkose (Zhao et al., 2016a). The Paleozoic formations are the Ordovician Duobaoshan and Wubinaobao formations, the Silurian Woduhe Formation, and the Carboniferous Hongshuiquan, Moergenhe, and Yigenhe formations. The Duobaoshan Formation is a suite of intermediate-acid volcanic rocks intercalated with shale and slate; the Wubinaobao Formation includes various slates with minor siltstone and limestone lenses; the Woduhe Formation consists of slate and sandstone; the Hongshuiquan Formation comprises a set of typical marine-facies clastics, limestone, and intercalated tuff; the Moergenhe Formation comprises marine intermediate-acidic volcanic rocks; and the Yigenhe Formation is a series of oceanic-continental facies clastic sediments. The Mesozoic deposits are continental volcanics and clastics. The Jurassic formations are the Nanping Formation, a set of conglomerates, sandstones, thin-bedded mudstones, and intercalated rhyolitic volcanic rocks; and the Tamulangou Formation, which includes basic and intermediate-basic volcanic rocks with minor pyroclastics. The Cretaceous stratigraphy includes the Jixiangfeng Formation, with Na-rich rhyolite and volcaniclastics; the Shangkuli Formation, which consists of rhyolitic and dacitic lavas and volcaniclastic rocks; and the Yiliekede Formation, which contains basalt, trachyandesite, trachyte, and intercalated rhyolitic volcanic (IMBGMR, 1996; Meng et al., 2011).

In the Erguna Massif, major NE-oriented faults (e.g., the Derbugan, Erguna River, and Genhe faults) dissect the massif and seem to control the Mesozoic volcanism and mineralization. There are also many NW- and NE-oriented extensional and torsional faults affiliated to these major faults (IMBGMR, 1996).

Multiple detailed studies have investigated the magmatic history of the Erguna Massif, and there is a large amount of published geochronological and geochemical data for this area. Tang et al. (2013) identified intrusions from four major Neoproterozoic magmatic events: (1) 851 Ma syenogranites in Shanghulin and southeast of Enhe; (2) a 792 Ma bimodal igneous assemblage of gabbro and syenogranite in southeast of Shiwe; (3) 762 Ma granodiorite intrusions located east of Shiwei; and (4) 737 Ma syenogranites found northeast of Enhe. Early Paleozoic magmatism occurred at 500–450 Ma. Representative plutons include the Alongshan (456 Ma), Guanhuzhan (464 Ma), Chalaban River (481–456 Ma), Mangui (482–480 Ma), Tahe (494–480 Ma), Halabaqi (500–

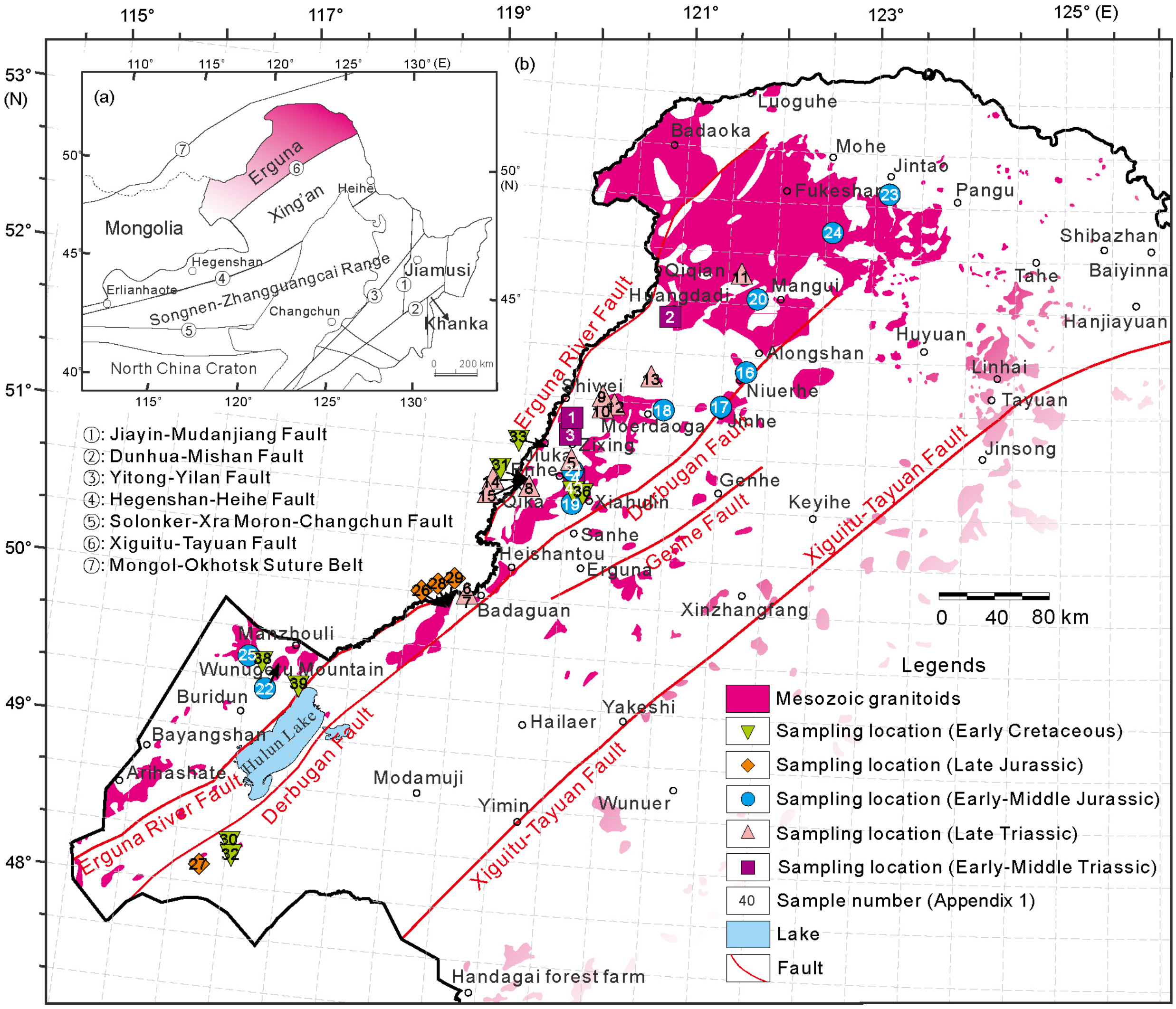

Figure 1 Distribution map of Mesozoic granitoids in the Erguna Massif. (a) Regional tectonic framework (modified after Wu et al., 2007). (b) Outcrops of granitoids and sampling locations.

461 Ma), Shibazhan (499 Ma), Ximenduli River (502 Ma), and Luogu River (517–504 Ma) plutons (Wu et al., 2005; Sui et al., 2006; Qin et al., 2007; Ge et al., 2007; Wu et al., 2011; Zhao et al., 2014). Late Paleozoic magmatisms can be subdivided into four stages (Zhao, 2011): (1) Late Devonian (383–372 Ma) calc-alkaline andesites, dacites, and rhyolites; (2) early Carboniferous (355–330 Ma) calc-alkaline gabbro, quartz diorite, and granodiorite (Zhou et al., 2005; Zhao et al., 2010); (3) late Carboniferous (320–300 Ma) granodiorites and monzogranites, most of which belong to the high-K calc-alkaline series (Wu et al., 2011), though a few are shoshonitic (Sui et al., 2009); and (4) Early-Middle Permian (290–260 Ma) alkaline granitoids (Hong et al., 1994; Sun et al., 2001; Wu et al., 2002). In the Mesozoic, the magmatism is dominated by granites and rhyolites, and can be subdivided into five stages: Early-Middle Triassic (247–241 Ma), Late Triassic (229–202 Ma), Early-Middle Jurassic (197–171 Ma), Late Jurassic (155–150 Ma), and Early Cretaceous (145–125 Ma) (Tang et al., 2014, 2015). In this study, we examined the Mesozoic granitoids in detail.

3. The episodes and distribution of Mesozoic granitoids in the Erguna Massif

Most of the granitoids in the Erguna Massif lie to the northwest of the Derbugan Fault (Figure 1b), especially to the north of Mangui and Qiqian. In the southwest Manzhouli area, granitoids crop out on Wunugetu and Bayang mountains, and in the central Erguna region they are located near Badaguan and within the Shanghulin and Enhe basins. In recent years, there is a wealth of published zircon U-Pb age data for Mesozoic granitoids of the Erguna Massif. Our research team's achievements are shown in Appendix 1 (available at http://earth.scichina.com), and those of other studies in Appendix 2.

The zircon U-Pb ages indicate nine episodes of granitic magmatism in the Erguna Massif (245, 225, 205, 195, 182, 174, 153, 145, and 124 Ma; Figure 2), which we have grouped into five main stages detailed below.

3.1 Early-Middle Triassic

Our zircon U-Pb dating results, together with previously published data, indicate that the earliest episode of Mesozoic granitic magmatism occurred in the Early-Middle Triassic (249–237 Ma) (Appendixes 1 and 2), with a peak age of 245 Ma (Figure 2). Granitoids of this age are found in the Enhe, Shiwei, Jiuka, West Niu'er River, Moerdaoga, Badaoka and Guanhuzhan areas in the Erguna Massif (Wu et al., 2011; She et al., 2012; Sun D Y et al., 2013; Tang et al., 2014, 2016). Granitic plutons with this peak age are also widespread throughout the Central Mongolia in the region to the southeast of the Mongol-Okhotsk suture belt. For example, there are Late Permian to Early-Middle Triassic granitic intrusions in the Hangayn area (Orolmaa et al., 2008). SHRIMP zircon U-Pb dating gives ages of 241±3 Ma for granites in the Tumurtin Ovoo zinc skarn deposit (Jiang et al., 2010b), and SHRIMP and LA-ICP-MS zircon U-Pb ages are in the range 247–240 Ma for quartz diorite and granodiorite from the Erdenet Cu-Mo porphyry deposit (Jiang et al., 2010a).

3.2 Late Triassic

The second episode of granitic magmatism occurred in the Late Triassic (229–201 Ma) (Appendixes 1 and 2), with peak ages at 225 and 205 Ma (Figure 2). The 225 Ma granitoids (granodiorites and syenogranites) are limited to the Manzhouli and Badaguan areas in the southwest part of the Erguna Massif (Tang et al., 2016); syenogranites with ages of 220±3 Ma occur northwest of Mangui and Tayuan (Wu et al., 2011). This episode of granitic magmatism also affected Central Mongolia; e.g., granitoids with ages of 228–230 Ma in the Nariyn Teel pluton and the Kharkhorin Massif (Yarmolyuk et al., 2002; Jahn et al., 2004). Granitoids with peak ages of 205 Ma are widespread throughout the Erguna Massif, at Mangui (Tang et al., 2016), Wunugetu Mountain (She et al., 2011), Moerdaoga (She et al., 2012; Tang et al., 2016), Alongshan (Wu et al., 2011), Qiqian (Sun D Y et al., 2013), the Taipingchuan Cu-Mo deposit (Chen et al., 2010), and the Kadajiling Pb-Zn deposit (She et al., 2011).

3.3 Early-Middle Jurassic

The third magmatic event that we identified occurred in the Early-Middle Jurassic (199–171 Ma) (Appendixes 1 and 2), with peak ages at 195, 182 and 174 Ma (Figure 2). Granitoids with peak ages of 195 Ma are found at Jinhe (Wu et al., 2011; Tang et al., 2016), western part of Mangui (Sun D Y et al., 2013), Xilinji (Wu et al., 2011), Moerdaoga (Wu et al., 2011; Tang et al., 2016) and Fukeshan (Wu et al., 2011) areas, etc; those with a peak age of 182 Ma are found at Lvlin (Wu et al., 2011), Pangu (Wu et al., 2011), Wunugetu Mountain (Wang W et al., 2012; She et al., 2012; Wang et al., 2014), Mohe (Sun D Y et al., 2013), Mangui (Wu et al., 2011), and Fukeshan (Sun D Y et al., 2013) areas, etc; and granitoids with a peak age of 174 Ma crop out at Mangui, Amuer, Chagantaolegai Mountain (Wang W et al., 2012), Wunugetu Mountain (She et al., 2012), and Dashimo (Wang et al., 2014) areas, etc.

3.4 Late Jurassic

The fourth magmatic episode occurred in the Late Jurassic (155–149 Ma) (Appendixes 1 and 2), with the peak age of 153 Ma (Figure 2). These granitoids occur mainly near Badaguan (Tang et al., 2015), Shiwei (Tang et al., 2016), Mangui (Sun D Y et al., 2013; Tang et al., 2015, 2016), Baogedewula (Wang W et al., 2012; Wang et al., 2014), and Arihashate (Wang et al., 2014) areas.

3.5 Early Cretaceous

The fifth episode of Mesozoic granitic magmatism occurred in the Early Cretaceous (145–125 Ma) (Appendixes 1 and 2). We subdivide this episode into two periods, with peak ages at 145 and 125 Ma (Figure 2). The 145 Ma period was the more intense of the two, and granitoids of this age are located in the areas near Qika (Tang et al., 2015), Wunugetu Mountain (She et al., 2012), Baogedewula (Wang W et al., 2012; Wang et al., 2014), and Arihashate (Wang et al., 2014). The 125 Ma granitoids consist of alkali-feldspar granite and monzogranite, and are only found at Niuer River (Wu et al., 2011) and Jiuka (Tang et al., 2015) areas. This Early Cretaceous magmatic event was different to the preceding episodes as it also involved the eruption of rhyolites, which occur mainly around Manzhouli. The published age data for these rhyolites (Appendix 1) indicate two stages of rhyolitic volcanism (dotted line in Figure 2): the first has a peak age of ~143 Ma and corresponds to the Jixiangfeng Formation, and the second has a peak age of ~125 Ma and corresponds to the Shangkuli

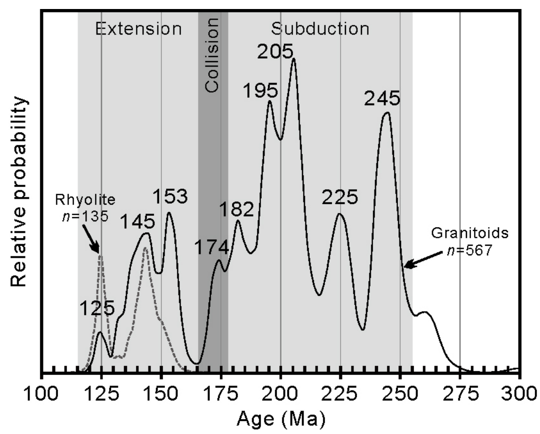

Figure 2 Relative probability plot of the zircon U-Pb ages for the Mesozoic granitoids within the Erguna Massif.

Formation.

4. Geochemistry and petrogenesis of Mesozoic granitoids in the Erguna Massif

The Mesozoic granitoids in the Erguna Massif in this study comprise a suite of granodiorite, monzogranite, and syenogranite (Appendix 1). In the TAS diagram, they fall in the fields of granodiorite and granite, and they belong to the subalkaline series (Figure 3). Zircon saturation temperatures of these granitoids were calculated using an equation for zircon solubility derived by Watson and Harrison (1983, 2005) from high-temperature (700–1300°C) experiments. The distribution coefficient of Zr ($D_{Zr}^{zircon/melt}$) is a function of the temperature and composition of the melt at the time that zircon is crystallizing from the granitic magma. When the activity coefficient is assumed to be 1, the zircon saturation temperature (T_{Zr}) can be calculated as follows:

$$T_{Zr}(°C) = \{12900 / [\ln D_{Zr}(496000 / \text{Melt}) + 0.85 \times M + 2.95]\} - 273.15, \quad (1)$$

where D_{Zr} is the ratio of the concentration of Zr in zircon to that in the melt, and M is the cation ratio (2Ca+K+Na)/(Si×Al) defined by Watson and Harrison (1983, 2005), calculated using host-rock-normalized concentrations. Without Zr and Hf correction, the Zr content in the pure zircon is 496000×10^{-6} ppm, and in general the Zr content of the melt is similar to that of the whole rock.

The zircon saturation temperatures of the Mesozoic granitoids can be subdivided into two series: an Early-Middle Triassic to Early-Middle Jurassic low-temperature series (< 825°C) and a Late Jurassic to Early Cretaceous high-temperature series (> 825°C) (Figure 4). This is consistent with the geochemical classification of the granitoids (Tang et al., 2014, 2015, 2016), with the low-temperature series being I-type granites and the high-temperature series being A-type granites.

The Mesozoic granitoids have similar major element compositions to each other (Figure 5). In contrast, some trace element concentrations and ratios vary with age (Figure 6), e.g., Sr/Y ratios, Eu/Eu* ratios, and Sr concentrations decrease with time, whereas Zr and Y concentrations increase. It is important to consider whether these patterns are a result of magmatic differentiation. Granitic magma has a high viscosity and can be described as crystal porridge (Pitcher, 1997). In addition, the time from magma formation to zircon U-Pb isotope system closure for a single pluton is usually less than 1 Myr (Petford et al., 2000; Glazner et al., 2004). This indicates that it may be difficult for fractional crystallization to take place (Zhang et al., 2007). We therefore assume that the Mesozoic granitoids in this study are representative of the primary magmas. Based on this assumption, we infer that geochemical differences between the coeval granitoids at different locations reflect lateral changes in the magma source region, and that the differences between granitoids emplaced in the same area but at different ages reveal vertical heterogeneity in the magma source region.

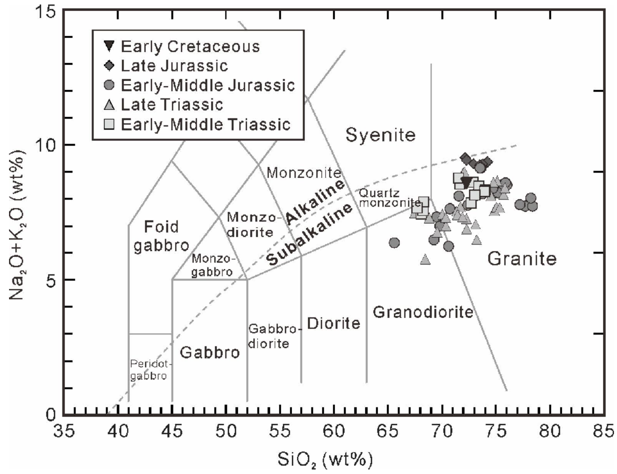

Figure 3 SiO_2 (wt%) versus (Na_2O+K_2O) (wt%) diagram for Mesozoic granitoids within the Erguna Massif. The field boundaries are from Maitre (1989).

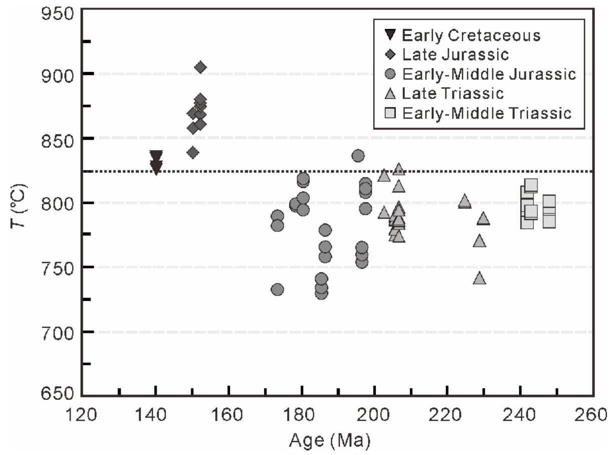

Figure 4 Plot of zircon saturation temperature versus age.

There is a linear correlation between the Sr/Y ratios of granitoids and crustal thickness (Girardi et al., 2012; Chapman et al., 2015; Chiaradia, 2015; Paterson and Ducea, 2015). The Sr/Y ratios of the Mesozoic granitoids in the Erguna Massif decrease with time (i.e., the youngest samples have the lowest ratios) (Figure 6a), suggesting continuous thinning of the continental crustal during the Mesozoic. There is further support for this inference as follows. (1) The Erguna Massif was affected by the southward subduction of the Mongol-Okhotsk oceanic plate during the early Mesozoic (Triassic-Early Jurassic), which resulted in crustal thickening in the Erguna Massif at that time (i.e., through the emplacement of adakitic rocks in an active continental margin setting) (Chen et al., 2010; Tang et al., 2016). (2) The presence of Middle Jurassic muscovite

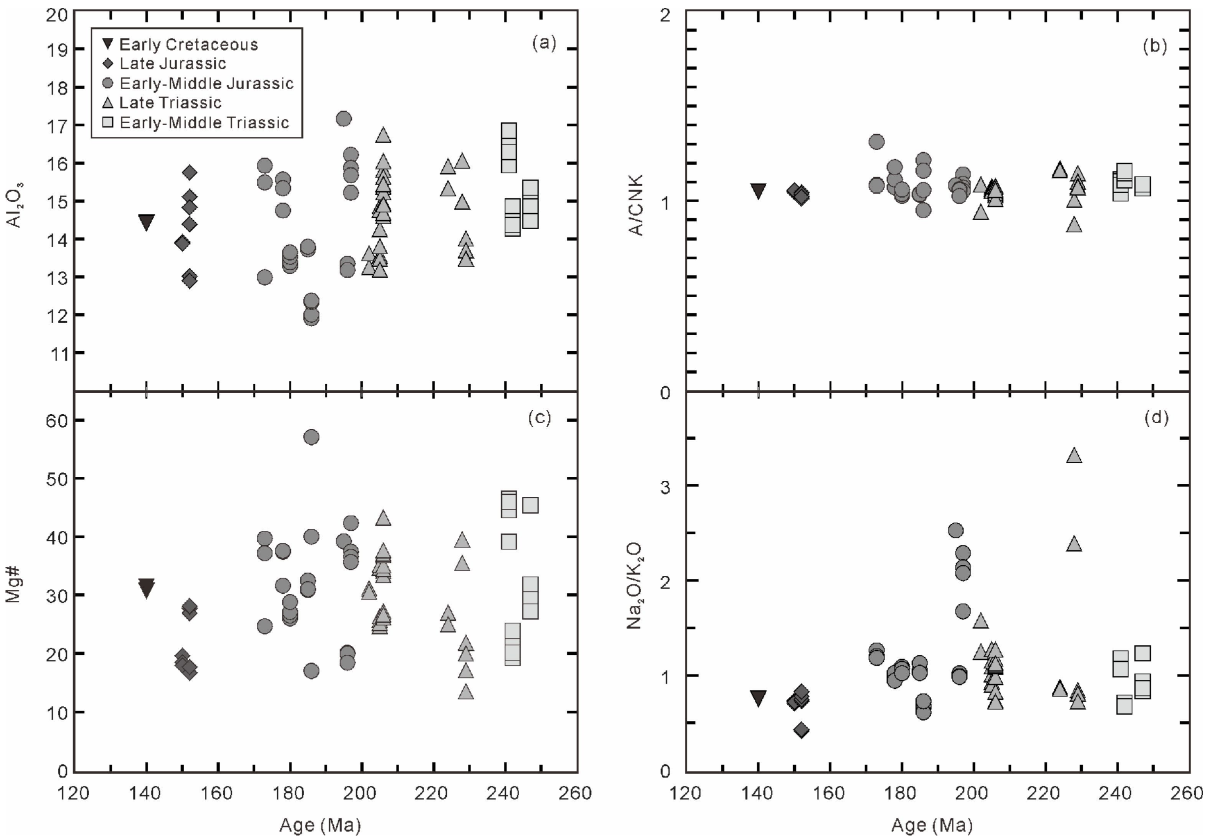

Figure 5 Plots of major element concentration against age for Mesozoic granitoids from the Erguna Massif.

granites, which have the geochemical signature of S-type granites, in the northern Great Xing'an Range provides evidence for the final closure of the Mongol-Okhotsk Ocean, a continent-continent collisional setting, and further thickening of the continental crust (Li et al., 2015). (3) The presence of the Late Jurassic to Early Cretaceous A-type granites and alkaline rhyolites indicates an extensional tectonic setting, and therefore thinning of the Erguna Massif. It should be noted that the $(La/Yb)_N$ ratios do not show the same pattern as the Sr/Y ratios (Figure 6c). However, previous studies indicate that high $(La/Yb)_N$ ratios may be affected by a number of other factors in addition to crustal thickness, including melting of thickened/delaminated lower continental crust (Atherton and Petford, 1993), fractional crystallization (Richards and Kerrich, 2007), magma mixing (Guo et al., 2007), as well as partial melting of granulite or enriched mantle (Jiang et al., 2007; Martin et al., 2005). These studies show that the $(La/Yb)_N$ ratios might be controlled by many factors rather than just related to the crustal thickness (Zhao, 2016). The Mesozoic granitoids also show an increasing concentration of Y with time (Figure 6e), reflecting the depletion of garnet in the magma source region and indicating a continuous thinning of the continental crust. Therefore, the variations of both Sr/Y ratios and Y concentrations with time reflect changes in crustal thickness, consistent with the regional tectonic history (Figure 2). Additionally, the decrease in both the Eu/Eu^* ratio and Sr concentration with time (Figure 6b and f) could be attributed to the crystallization of plagioclase, as both elements substitute into this mineral (Girardi et al., 2012).

The Mesozoic granitoids have high concentrations of SiO_2 (>65%) and Al_2O_3, and low concentrations of $Mg^{\#}$, TFe_2O_3, Cr, Co and Ni, this precludes any mixing of the granitic melts with mantle-derived magma (Lu and Xu, 2011). This observation, together with the enrichment in light rare-earth elements (LREEs) and large ion lithophile elements (LILEs), depletion in heavy rare-earth elements (HREEs) and high field-strength elements (HFSEs), as well as high $(La/Yb)_N$ values (average at 23.0), indicates that the primary magmas for the Mesozoic granitoids were derived from partial melting of the lower continental crust (Xu et al., 2009; Tang et al., 2014, 2015, 2016).

5. Zircon Hf isotopic compositions of Mesozoic granitoids in the Erguna Massif

This paper summarizes the results of several years of zircon Hf isotopic analysis, and data references are shown in Appendix 1. Additional zircon Hf isotopic data, measured from samples of Middle Jurassic age and younger, are presented in Appendix 3. Due to the uncertainties of Hf isotopic measurements of captured zircons, we only discuss the Hf isotopic

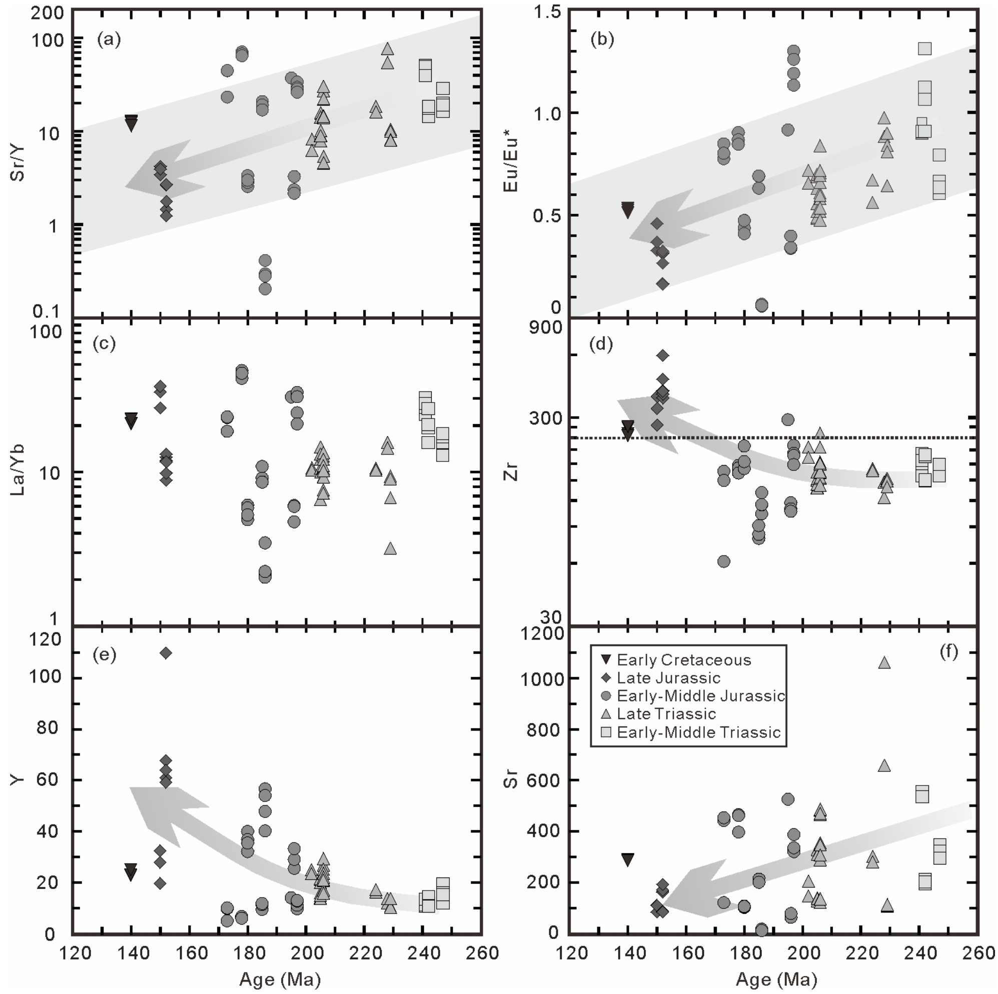

Figure 6 Plots of the concentration of trace elements against age for Mesozoic granitoids in the Erguna Massif.

compositions of zircons for which we also obtained crystallization ages.

5.1 Hf isotope analysis

Using zircon LA-ICP-MS U-Pb dating results, together with zircon CL images, we analyzed the Hf isotopic compositions of zircons sampled from granitoids of Middle Jurassic age and younger. In situ zircon Lu-Hf isotope analyses were conducted using a Neptune multi-collector ICP-MS (MC-LA-ICPMS) in combination with a Geolas 2005 excimer ArF laser ablation system (193 nm) that was hosted at the Institute of Geology and Geophysics, Chinese Academy of Sciences. All data were acquired on zircon in single spot ablation mode with a spot size of 44 μm, pulse width of 15 ns, laser pulse frequency of 8–10 Hz, and laser pulse energy of 100 mJ. The ablated aerosol was carried by helium, and 91500 served as the external standard. For details of the operating conditions for the laser ablation systemand the MC-ICP-MS instrument, as well as the analytical method, see Xu et al. (2004) and Wu et al. (2006). The results are presented in Appendix 3. It should be noted that the average crustal value (−0.5482) is used as the standard data to analyze the zircon Lu-Hf results in this paper.

5.2 Zircon Hf isotopic compositions of Mesozoic granitoids in the Erguna Massif

Nearly all zircon Hf isotopic data from different stages of Mesozoic granitoids in different areas fall in the field of the eastern segment of CAOB in Figure 7a, similar to those of zircons from the Phanerozoic igneous rocks in the Xing-Meng Orogenic Belt (XMOB), obviously different from those of zircons from Paleozoic-Mesozoic units within the Yanshan Fold and Thrust Belt (YFTB) (Xiao et al., 2004; Yang et al., 2006).

(1) Early-Middle Triassic granitoids. The Early-Middle Triassic granitiods mainly formed at ~241, ~242, ~246 and ~247 Ma. Two dispersed data from the 247 Ma granitoids were discarded because we obtained a wide range of Hf

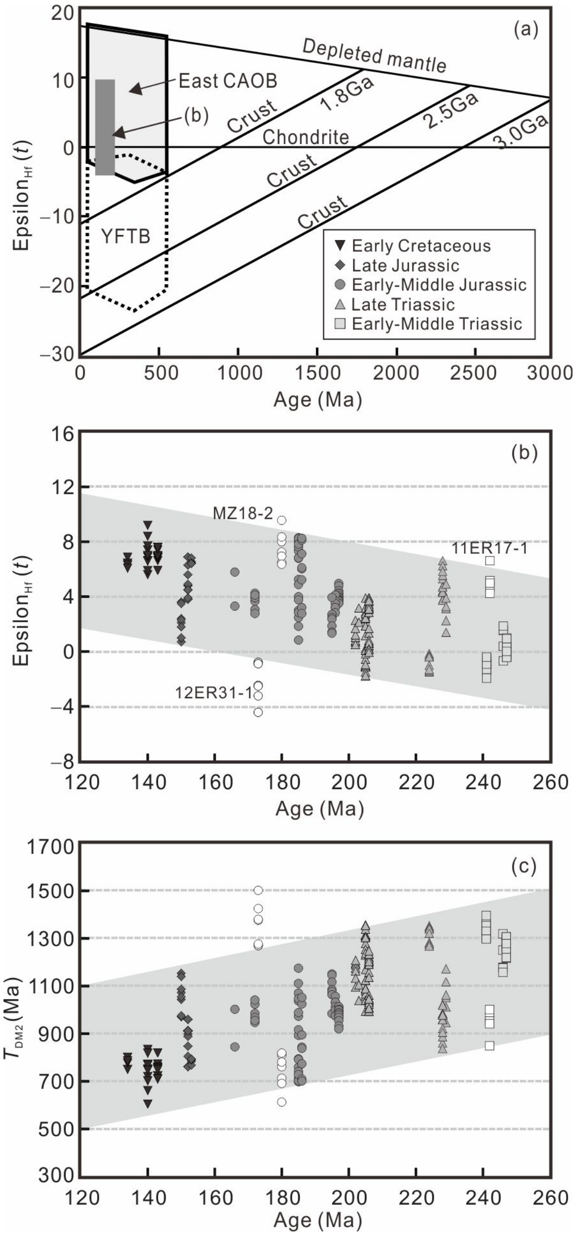

Figure 7 Plots of zircon Hf isotopic composition against age. (a) Correlations between zircon $\varepsilon_{Hf}(t)$ value and age (modified after Yang et al., 2006). (b) Detailed plot of zircon $\varepsilon_{Hf}(t)$ value against age. (c) Detailed plot of zircon T_{DM2} age against age.

isotopic data. The dispersed data may arise because the zircons contained inclusions, or because they had experienced magma mixing. The initial $^{176}Hf/^{177}Hf$ ratios for 32 zircons vary from 0.282570 to 0.282817. Their $\varepsilon_{Hf}(t)$ values and T_{DM2} ages range from −2.0 to 6.6 (Figure 7b) and from 849 to 1395 Ma (Figure 7c), respectively. The average T_{DM2} age is 1231 Ma.

(2) Late Triassic granitoids. The Late Triassic granitiods mainly formed at ~202, ~203, ~205, ~206, ~224, ~228 and ~229 Ma. The initial $^{176}Hf/^{177}Hf$ ratios for 86 zircons vary from 0.282597 to 0.282821. Their $\varepsilon_{Hf}(t)$ values and T_{DM2} ages range from –1.8 to +6.6 (Figure 7b) and from 838 to 1357 Ma (Figure 7c), respectively. The average T_{DM2} age is 1124 Ma.

(3) Early-Middle Jurassic granitoids. The Early-Middle Jurassic granitoids mainly formed at ~171, ~173, ~180, ~185, ~186, ~195, ~196 and ~197 Ma. Seven dispersed zircon Hf isotopic data among these granitoids were discarded. The initial $^{176}Hf/^{177}Hf$ ratios for 73 zircons vary from 0.282541 to 0.282940. Their $\varepsilon_{Hf}(t)$ values and T_{DM2} ages range from –4.4 to 9.6 (Figure 7b) and from 613 to 1501 Ma (Figure 7c), respectively. The average T_{DM2} age is 971 Ma.

(4) Late Jurassic granitoids. The Late Jurassic granitiods mainly formed at ~150, ~152, and ~153 Ma. Two dispersed zircon Hf isotopic data from 153 Ma granitoids were discarded. The initial $^{176}Hf/^{177}Hf$ ratios for 24 zircons vary from 0.282701 to 0.282877. Their $\varepsilon_{Hf}(t)$ values and T_{DM2} ages range from 0.7 to 6.9 (Figure 7b) and from 761 to 1154 Ma (Figure 7c), respectively. The average T_{DM2} age is 919 Ma.

(5) Early Cretaceous granitoids. The Early Cretaceous granitoids mainly formed at ~134, ~140, and ~145 Ma. The initial $^{176}Hf/^{177}Hf$ ratios for 24 zircons vary from 0.282847 to 0.282952. Their $\varepsilon_{Hf}(t)$ values and T_{DM2} ages range from 5.6 to 9.2 (Figure 7b) and from 604 to 834 Ma (Figure 7c), respectively. The average T_{DM2} age is 750 Ma.

6. Spatial-temporal variations of zircon Hf isotopic compositions and crustal accretion and reworking processes

6.1 Temporal variation in zircon Hf isotopic compositions

Based on the statistics of zircon Hf isotopic data of the Mesozoic granitioids in the Erguna Massif, it is found that their zircon $\varepsilon_{Hf}(t)$ values gradually increase (Figure 7b), whereas the T_{DM2} ages gradually decrease (from Mesoproterozoic to Neoproterozoic) (Figure 7c) with decreasing of their ages. The correlation between zircon Hf isotopic data and the formation time of granitoids suggests a change in the source of magmas from the melting of ancient crust to juvenile crust, during the Mesozoic. However, some zircon Hf isotopic data (white circles and squares in Figure 7b and c) deviate from this overall trend, possibly because of lateral heterogeneity in the source region of granitic magma (Figure 8).

6.2 Spatial variation in zircon Hf isotopic compositions

The zircon $\varepsilon_{Hf}(t)$ values of the Mesozoic granitoids in the Erguna Massif gradually decrease northward, indicating that, moving from south to north, there is an increasing component of ancient crustal material within the lower continental crust. This interpretation is supported by the presence of outcrops of Neoproterozoic and Paleoproterozoic plutons in the northeast of the Erguna Massif (She et al., 2012; Tang et al., 2013; Sun L X et al., 2013; Shao et al., 2015; Zhao et al., 2016a, 2016c). Additionally, at same latitude there is a wide range in zircon Hf isotopic compositions (grey texture region in Figure 8). Taken together, these observations suggest both lateral and vertical heterogeneities in the lower continental crust of the Erguna Massif during the Mesozoic.

6.3 Crustal accretion and reworking processes

Recent studies have identified some ancient basement rocks within the Erguna Massif. For examples, Sun L X et al. (2013) reported that the Paleoproterozoic granitic gneisses in the north of Hanjiayuan town in the Erguna Massif with zircon $^{207}Pb/^{206}Pb$ ages of 1837±5, 1741±30, and 1854±20 Ma, zircon $\varepsilon_{Hf}(t)$ values of −3.9 to −8.5, and T_{DM2} ages of 2.78 to 3.01 Ga. The gneissic monzogranites with zircon $^{207}Pb/^{206}Pb$ ages of 2606±17 Ma have been discovered from Bilieya Pb-Zn deposit in the Erguna Massif (Shao et al., 2015). Moreover, some T_{DM2} ages of the Neoproterozoic granites from Mangui area are older than 2000 Ma (Zhao et al., 2016b). In summary, there is a Paleoproterozoic and even Archaeozoic basement in the Erguna Massif, but these basement rocks are of minor extent because the primary continental crust has been reworked multiple times during the complex tectonic history of the CAOB.

Based on the relative probability of zircon T_{DM2} ages of the Mesozoic granitoids within the Erguna massif (Figure 9), the growth of continental crust in the eastern segment of CAOB occurred in three stages: Mesoproterozoic, late Mesoproterozoic-early Neoproterozoic, and Neoproterozoic, much earlier than the Phanerozoic, as previously considered (Wu et al., 1999, 2011).

The zircon Hf isotopic compositions of Mesozoic granitoids reveal that the accretion of lower continental crust in the Erguna micro-continental Massif mainly occurred in the Mesoproterozoic and Neoproterozoic. Then, it is important to reveal the reworking processes of the lower continental crust in this region, i.e., whether different generations of Mesozoic granitoids were derived from the same or different source rocks. Considering the relationship between zircon ages and T_{DM2} ages (Figure 7c), and the variation in $\varepsilon_{Hf}(t)$ values with latitude (Figure 8), we suggest that in the northeast of the Erguna Massif, the Early-Middle Triassic granitoids were derived from Mesoproterozoic source rocks, the Late Jurassic and Early Cretaceous granitoids in the southwest Erguna Massif were derived from Neoproterozoic source rocks, and the Late Jurassic granitoids of the central Erguna Massif were derived from late Mesoproterozoic source rocks. Taken together, as the result of reworking process, the Mesozoic granitoids in the Erguna Massif were derived from the source rocks with different ages in different parts of the lower continental crust.

Based on the lateral and vertical heterogeneities of the lower continental crust within the Erguna Massif, as well as the accretion and reworking processes, we present a structural model of the lower continental crust of the Erguna Massif in Figure 10. In the model, the continental crust of the Erguna Massif was mainly formed by the underplating of mantle-derived magma. During the Mesozoic, partial melting of the lower crust generated granitic magmas at various depths, which migrated upwards, intruding into the upper crust and finally forming the widespread Mesozoic granitoids now exposed within the Erguna Massif.

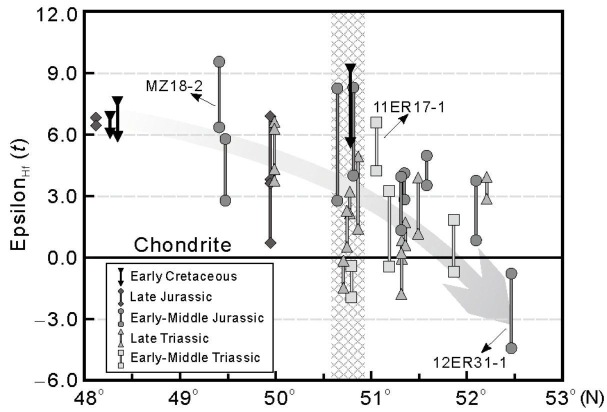

Figure 8 Latitude of sampling locations against $\varepsilon_{Hf}(t)$ values.

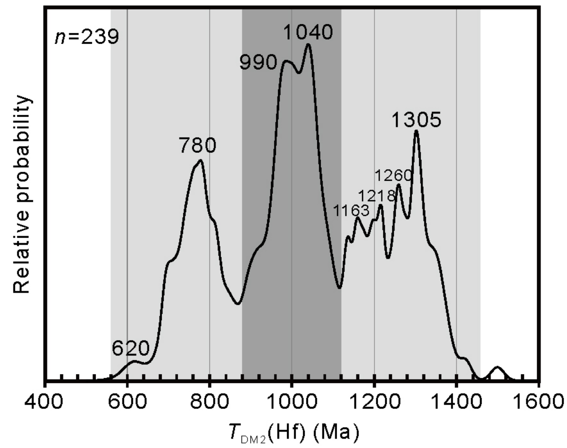

Figure 9 Relative probability of zircon T_{DM2} ages for the Mesozoic granitoids in the Erguna Massif.

7. Conclusions

(1) There are nine episodes of Mesozoic granitic magmatism in the Erguna massif (245, 225, 205, 195, 182, 174, 153, 145, and 124 Ma), which could be subdivided into five main stages: Early-Middle Triassic, Late Triassic, Early-Middle Jurassic, Late Jurassic and Early Cretaceous.

(2) Sr/Y and Eu/Eu* ratios and Sr concentrations decrease with time (i.e., with decreasing age of granitoid), while Zr

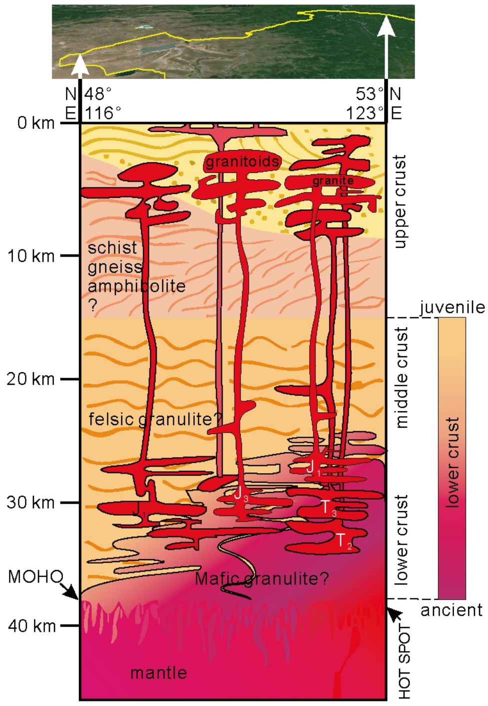

Figure 10 Structural model of lower continental crust within the Erguna massif. Modified after Hawkesworth and Kemp (2006), Cawood et al. (2013) and Roberts et al. (2015).

and Y concentrations increase. These patterns indicate that the Erguna Massif experienced crustal thickening followed by thinning, and that increasing amounts of plagioclase crystallized from the magma during this time.

(3) The zircon Hf isotopic compositions indicate that the accretion of the lower continental crust within the Erguna Massif mainly happened in the Mesoproterozoic and Neoproterozoic.

(4) The formation of Mesozoic granitoids in the Erguna Massif reveals the reworking process of the lower continental crust, i.e., under the control of the southward subduction, collision, and post-collisional extension of the Mongol-Okhotsk oceanic plate, there was a change in the source of the granitic magmas from partial melting of ancient crust to juvenile crust.

Acknowledgements *Thanks to the reviewers' comments and suggestions, it is very important to improve the quality of this paper. We also thank the staff of the State Key Laboratory of Geological Processes and Mineral Resources, China University of Geosciences, Wuhan, China, and the Institute of Geology and Geophysics, Chinese Academy of Sciences, Beijing, China, for their advice and assistance during U-Pb zircon dating, major and trace element analyses, and Hf isotope analysis. This work was supported by the MOST of China (Grant No. 2016YFC0600403) and the National Natural Science Foundation of China (Grant No. 41330206).*

References

Atherton M P, Petford N. 1993. Generation of sodium-rich magmas from newly underplated basaltic crust. Nature, 362: 144–146

Belousova E A, Kostitsyn Y A, Griffin W L, Begg G C, O'Reilly S Y, Pearson N J. 2010. The growth of the continental crust: Constraints from zircon Hf-isotope data. Lithos, 119: 457–466

Campbell I H, Taylor S R. 1983. No water, no granites—No oceans, no continents. Geophys Res Lett, 10: 1061–1064

Cao H H, Xu W L, Pei F P, Wang Z W, Wang F, Wang Z J. 2013. Zircon U-Pb geochronology and petrogenesis of the Late Paleozoic-Early Mesozoic intrusive rocks in the eastern segment of the northern margin of the North China Block. Lithos, 170-171: 191–207

Cawood P A, Hawkesworth C J, Dhuime B. 2013. The continental record and the generation of continental crust. Geol Soc Am Bull, 125: 14–32

Chapman J B, Ducea M N, DeCelles P G, Profeta L. 2015. Tracking changes in crustal thickness during orogenic evolution with Sr/Y: An example from the North American Cordillera. Geology, 43: 919–922

Chen Z G, Zhang L C, Lu B Z, Li Z L, Wu H Y, Xiang P, Huang S W. 2010. Geochronology and geochemistry of the Taipingchuan copper-molybdenum deposit in Inner Mongolia, and its geological significances (in Chinese). Acta Petrol Sin, 26: 1437–1449

Chiaradia M. 2015. Crustal thickness control on Sr/Y signatures of recent arc magmas: An Earth scale perspective. Sci Rep, 5: 8115

DePaolo D J, Linn A M, Schubert G. 1991. The continental crustal age distribution: Methods of determining mantle separation ages from Sm-Nd isotopic data and application to the southwestern United States. J Geophys Res, 96: 2071–2088

Dhuime B, Hawkesworth C, Cawood P. 2011. When continents formed. Science, 331: 154–155

Dhuime B, Hawkesworth C J, Cawood P A, Storey C D. 2012. A change in the geodynamics of continental growth 3 billion years ago. Science, 335: 1334–1336

Dong Y, Ge W C, Yang H, Zhao G C, Wang Q H, Zhang Y L, Su L. 2014. Geochronology and geochemistry of Early Cretaceous volcanic rocks from the Baiyingaolao Formation in the central Great Xing'an Range, NE China, and its tectonic implications. Lithos, 205: 168–184

Ge W C, Li X H, Lin Q, Sun D Y, Wu F Y, Yun S Y. 2001. Geochemistry of Early Cretaceous alkaline rhyolites from Hulun Lake, Daxing'anling and its tectonic implications (in Chinese). Chin J Geol, 36: 176–183

Ge W C, Wu F Y, Zhou C Y, Zhang J H. 2007. Porphyry Cu-Mo deposits in the eastern Xing'an-Mongolian Orogenic Belt: Mineralization ages and their geodynamic implications. Chin Sci Bull, 52: 3416–3427

Girardi J D, Patchett P J, Ducea M N, Gehrels G E, Cecil M R, Rusmore M E, Woodsworth G J, Pearson D M, Manthei C, Wetmore P. 2012. Elemental and isotopic evidence for granitoid genesis from deep-seated sources in the coast mountains batholith, British Columbia. J Petrol, 53: 1505–1536

Glazner A F, Bartley J M, Coleman D S, Gray W, Taylor R Z. 2004. Are plutons assembled over millions of years by amalgamation from small magma chambers? Gsa Today, 14: 4–11

Guo F, Fan W M, Gao X F, Li C W, Miao L C, Zhao L, Li H X. 2010. Sr-Nd-Pb isotope mapping of Mesozoic igneous rocks in NE China: Constraints on tectonic framework and Phanerozoic crustal growth. Lithos, 120: 563–578

Guo F, Nakamuru E, Fan W, Kobayoshi K., Li C. 2007. Generation of palaeocene adakitic andesites by magma mixing: Yanji Area, NE China. J Petrol, 48: 41–55

Hawkesworth C J, Kemp A I S. 2006. The differentiation and rates of generation of the continental crust. Chem Geol, 226: 134–143

Hong D W, Huang H Z, Xiao Y J, Xu H M, Jin M Y. 1994. The Permian alkaline granites in Central Inner Mongolia and their geodynamic significance (in Chinese). Acta Geol Sin, 68: 219–230

Inner Mongolian Bureau of Geology Mineral Resources (IMBGMR). 1996. Lithostratigraphy of Inner Mongolia (in Chinese). Wuhan: China University of Geosciences Press. 342

Jacobsen S B. 1988. Isotopic and chemical constraints on mantle-crust evolution. Geochim Cosmochim Acta, 52: 1341–1350

Jahn B, Capdevila R, Liu D Y, Vernon A, Badarch G. 2004. Sources of Phanerozoic granitoids in the transect Bayanhongor-Ulaan Baatar, Mongolia: Geochemical and Nd isotopic evidence, and implications for Phanerozoic crustal growth. J Asian Earth Sci, 23: 629–653

Jahn B M, Wu F Y, Chen B. 2000a. Massive granitoid generation in central Asia: Nd isotopic evidence and implication for continental growth in the Phanerozoic. Episodes, 23: 82–92

Jahn B, Wu F Y, Chen B. 2000b. Granitoids of the Central Asian Orogenic Belt and continental growth in the Phanerozoic. Trans R Soc Edinb-Earth Sci, 91: 181–193

Jahn B M, Wu F Y, Hong D. 2000c. Important crustal growth in the Phanerozoic: Isotopic evidence of granitoids from east-central Asia. J Earth Syst Sci, 109: 5–20

Jiang N, Liu Y, Zhou W, Yang J, Zhang S. 2007. Derivation of Mesozoic adakitic magmas from ancient lower crust in the North China craton. Geochim Cosmochim Acta, 71: 2591–2608

Jiang S H, Nie F J, Su Y J, Bai D M, Liu Y F. 2010a. Geochronology and origin of the Erdenet superlarge Cu-Mo deposit in Mongolia (in Chinese). Acta Geosci Sin, 31: 289–306

Jiang S H, Nie F J, Su Y J, Cai J X, Ding Z. 2010b. The geological features and origin of the Tumurtin Ovoo large-scale Zinc deposit, Mongolia (in Chinese). Acta Geosci Sin, 31: 321–330

Li J Y, Niu B G, Song B. 1999. Crustal Formation and Evolution of Nothern Changbai Mountains (in Chinese). Beijing: Geological Publishing House. 137

Li J Y. 2006. Permian geodynamic setting of Northeast China and adjacent regions: Closure of the Paleo-Asian Ocean and subduction of the Paleo-Pacific Plate. J Asian Earth Sci, 26: 207–224

Li Y, Ding L L, Xu W L, Wang F, Tang J, Zhao S, Wang Z J. 2015. Geochronology and geochemistry of muscovite granite in Sunwu area, NE China: Implications for the timing of closure of the Mongol-Okhotsk Ocean (in Chinese). Acta Petrol Sin, 31: 56–66

Li Y, Xu W L, Wang F, Tang J, Pei F P, Wang Z J. 2014. Geochronology and geochemistry of late Paleozoic volcanic rocks on the western margin of the Songnen-Zhangguangcai Range Massif, NE China: Implications for the amalgamation history of the Xing'an and Songnen-Zhangguangcai Range massifs. Lithos, 205: 394–410

Liu W, Siebel W, Li X J, Pan X F. 2005. Petrogenesis of the Linxi granitoids, northern Inner Mongolia of China: Constraints on basaltic underplating. Chem Geol, 219: 5–35

Lu L Z, Xu W L. 2011. Petrography (in Chinese). Beijing: Geological Publishing House. 377

Maitre R W L. 1989. A Classification of Igneous Rocks and Glossary of terms: Recommendations of the International Union of Geological Sciences Subcommission on the Systematics of Igneous Rocks. Oxford: Blackwell Scientific Publications. 193

Martin H, Smithies R H, Rapp R, Moyen J F, Champion D. 2005. An overview of adakite, tonalite-trondhjemite-granodiorite (TTG), and sanukitoid: Relationships and some implications for crustal evolution. Lithos, 79: 1–24

Meng E, Xu W L, Pei F P, Yang D B, Yu Y, Zhang X Z. 2010. Detrital-zircon geochronology of Late Paleozoic sedimentary rocks in eastern Heilongjiang Province, NE China: Implications for the tectonic evolution of the eastern segment of the Central Asian Orogenic Belt. Tectonophysics, 485: 42–51

Meng E, Xu W L, Yang D B, Qiu K F, Li C H, Zhu H T. 2011. Zircon U-Pb chronology, geochemistry of Mesozoic volcanic rocks from the Lingquan basin in Manzhouli area, and its tectonic implications (in Chinese). Acta Petrol Sin, 27: 1209–1226

Orolmaa D, Erdenesaihan G, Borisenko A S, Fedoseev G S, Babich V V, Zhmodik S M. 2008. Permian-Triassic granitoid magmatism and metallogeny of the Hangayn (central Mongolia). Rus Geol Geophys, 49: 534–544

Paterson S R, Ducea M N. 2015. Arc magmatic tempos: Gathering the evidence. Elements, 11: 91–98

Petford N, Cruden A R, McCaffrey K J W, Vigneresse J L. 2000. Granite magma formation, transport and emplacement in the Earth's crust. Nature, 408: 669–673

Pitcher W S. 1997. The Nature and Origin of Granite. 2nd ed. London: Chapman & Hall. 358

Qin X F, Yin Z G, Wang Y, Guo Y S, Liu X G, Zhou S Q. 2007. Early paleozoic adakitic rocks in mohe area at the northern end of the da hinggan mountains and their geoligical significance (in Chinese). Acta Petrol Sin, 23: 1501–1511

Richards J P, Kerrich R. 2007. Special paper: Adakite-like rocks: Their diverse origins and questionable role in metallogenesis. Econ Geol, 102: 537–576

Roberts N M W, Van Kranendonk M J, Parman S, Clift P D. 2015. Continent formation through time. Geol Soc Lond Spec Publ, 389: 1–16

Rudnick R L. 1995. Making continental crust. Nature, 378: 571–578

Shao J, Li Y F, Zhou Y H, Wang H B, Zhang J. 2015. Neo-Archaean magmatic event in Erguna Massif of northeast China: Evidence from the zircon LA-ICP-MS dating of the gneissic monzogranite from the drill (in Chinese). J Jilin Univ-Earth Sci Ed, 45: 364–373

She H Q, Li J W, Xiang A P, Guan J D, Yang Y C, Zhang D Q, Tan G, Zhang B. 2012. U-pb ages of the zircons from primary rocks in middle-northern daxinganling and its implications to geotectonic evolution (in Chinese). Acta Petrol Sin, 28: 571–594

She H Q, Liang Y W, Li J W, Guan J D, Zhang D Q, Yang Y C, Xiang A P, Jin J, Tan G, Zhang B. 2011. The Early-Mesozoic magmatic activity at Moerdaoga district in Inner Mongolia and its geodynamic implication (in Chinese). J Jilin Univ-Earth Sci Ed, 41: 1831–1864

Sui Z M, Ge W C, Wu F Y, Xu X C, Wang Q H. 2006. U-Pb chronology in zircon from Harabaqi granitic pluton in northeastern Daxing' anling area and its origin (in Chinese). Glob Geol, 25: 229–236

Sui Z M, Ge W C, Xu X C, Zhang J H. 2009. Characteristics and geological implications of the Late Paleozoic post-orogenic Shierzhan granite in the Great Xing'an Range (in Chinese). Acta Petrol Sin, 25: 2679–2686

Sun D Y, Gou J, Wang T H, Ren Y S, Liu Y J, Guo H Y, Liu X M, Hu Z C. 2013. Geochronological and geochemical constraints on the Erguna massif basement, NE China-subduction history of the Mongol-Okhotsk oceanic crust. Int Geol Rev, 55: 1801–1816

Sun D Y, Wu F Y, Li H M, Lin Q. 2001. Emplacement age of the postorogenic A-type granites in Northwestern Lesser Xing'an Ranges, and its relationship to the eastward extension of Suolushan-Hegenshan-Zhalaite collisional suture zone. Chin Sci Bull, 46: 427–432

Sun L X, Ren B F, Zhao F Q, Ji S P, Geng J Z. 2013. Late Paleoproterozoic magmatic records in the Erguna massif: Evidences from the zircon U-Pb dating of granitic gneisses (in Chinese). Geol Bull China, 32: 341–352

Tang J, Xu W L, Wang F, Wang W, Xu M J, Zhang Y H. 2013. Geochronology and geochemistry of Neoproterozoic magmatism in the Erguna Massif, NE China: Petrogenesis and implications for the breakup of the Rodinia supercontinent. Precambrian Res, 224: 597–611

Tang J, Xu W L, Wang F, Wang W, Xu M J, Zhang Y H. 2014. Geochronology and geochemistry of Early-Middle Triassic magmatism in the Erguna Massif, NE China: Constraints on the tectonic evolution of the Mongol-Okhotsk Ocean. Lithos, 184-187: 1–16

Tang J, Xu W L, Wang F, Zhao S, Li Y. 2015. Geochronology, geochemistry, and deformation history of Late Jurassic-Early Cretaceous intrusive rocks in the Erguna Massif, NE China: Constraints on the late Mesozoic tectonic evolution of the Mongol-Okhotsk orogenic belt. Tectonophysics, 658: 91–110

Tang J, Xu W L, Wang F, Zhao S, Wang W. 2016. Early Mesozoic southward subduction history of the Mongol-Okhotsk oceanic plate: Evidence from geochronology and geochemistry of Early Mesozoic intrusive rocks in the Erguna Massif, NE China. Gondwana Res, 31: 218–240

Taylor S R, Mclennan S M. 1985. The Continental Crust: Its Composition and Evolution, an Examination of the Geochemical Record Preserved in Sedimentary Rocks. Oxford: Blackwell Scientific Publications. 312

Wang F, Xu W L, Gao F H, Meng E, Cao H, Zhao L, Yang Y. 2012a. Tectonic history of the Zhangguangcailing Group in eastern Heilongjiang Province, NE China: Constraints from U-Pb geochronology of detrital and magmatic zircons. Tectonophysics, 566-567: 105–122

Wang F, Xu W L, Meng E, Cao H H, Gao F H. 2012b. Early Paleozoic amalgamation of the Songnen-Zhangguangcai Range and Jiamusi massifs in the eastern segment of the Central Asian Orogenic Belt: Geochronological and geochemical evidence from granitoids and rhyolites. J Asian Earth Sci, 49: 234–248

Wang F, Xu W L, Xu Y G, Gao F, Ge W. 2015. Late Triassic bimodal igneous rocks in eastern Heilongjiang Province, NE China: Implications for the initiation of subduction of the Paleo-Pacific Plate beneath Eurasia. J Asian Earth Sci, 97: 406–423

Wang T H, Zhang S Y, Sun D Y, Gou J, Ren Y S, Wu P F, Liu X M. 2014. Zircon U-Pb ages and Hf isotopic characteristics of Mesozoic granitoids from southern Manzhouli, Inner Mongolia (in Chinese). Glob Geol, 33: 26–38

Wang W, Xu W L, Wang F, Meng E. 2012. Zircon U-Pb chronology and assemblages of Mesozoic granitoids in the Manzhouli-Erguna area, NE China: Constraints on the regional tectonic evolution (in Chinese). Geol J China Univer, 18: 88–105

Watson E B, Harrison T M. 1983. Zircon saturation revisited: Temperature and composition effects in a variety of crustal magma types. Earth Planet Sci Lett, 64: 295–304

Watson E B, Harrison T M. 2005. Zircon thermometer reveals minimum melting conditions on earliest Earth. Science, 308: 841–844

Windley B F, Alexeiev D, Xiao W, Kroner A, Badarch G. 2007. Tectonic models for accretion of the central Asian orogenic belt. J Geol Soc, 164: 31–47

Windley B F, Allen M B, Zhang C, Zhao Z Y, Wang G R. 1990. Paleozoic accretion and Cenozoic redeformation of the Chinese Tien Shan Range, central Asia. Geology, 18: 128–131

Wu F Y, Jahn B, Wilde S A, Lo C H, Yui T F, Lin Q, Ge W C, Sun D Y. 2003. Highly fractionated I-type granites in NE China (II): Isotopic geochemistry and implications for crustal growth in the Phanerozoic. Lithos, 67: 191–204

Wu F Y, Jahn B, Wilde S, Sun D Y. 2000. Phanerozoic crustal growth: U-Pb and Sr-Nd isotopic evidence from the granites in northeastern China. Tectonophysics, 328: 89–113

Wu F Y, Sun D Y, Ge W C, Zhang Y B, Grant M L, Wilde S A, Jahn B M. 2011. Geochronology of the Phanerozoic granitoids in northeastern China. J Asian Earth Sci, 41: 1–30

Wu F Y, Sun D Y, Li H M, Jahn B, Wilde S. 2002. A-type granites in northeastern China: Age and geochemical constraints on their petrogenesis. Chem Geol, 187: 143–173

Wu F Y, Sun D Y, Lin Q. 1999. Petrogenesis of the Phanerozoic granites and crustal growth in Northeast China (in Chinese). Acta Petrol Sin, 15: 181–189

Wu F Y, Yang Y H, Xie L W, Yang J H, Xu P. 2006. Hf isotopic compositions of the standard zircons and baddeleyites used in U-Pb geochronology. Chem Geol, 234: 105–126

Wu F Y, Zhao G C, Sun D Y, Wilde S A, Yang J H. 2007. The Hulan Group: Its role in the evolution of the Central Asian orogenic belt of NE China. J Asian Earth Sci, 30: 542–556

Wu G, Sun F Y, Zhao C S, Li Z T, Zhao A L, Pang Q B, Li G Y. 2005. Discovery of the Early Paleozoic post-collisional granites in northern margin of the Erguna massif and its geological significance. Chin Sci Bull, 50: 2733–2743

Xiao W J, Windley B F, Hao J, Zhai M G. 2003. Accretion leading to collision and the Permian Solonker suture, Inner Mongolia, China: Termination of the central Asian orogenic belt. Tectonics, 22: 1069

Xiao W J, Zhang L C, Qin K Z, Sun S, Li J L. 2004. Paleozoic accretionary and collisional tectonics of the eastern Tianshan (China): Implications for the continental growth of central Asia. Am J Sci, 304: 370–395

Xu M J, Xu W L, Wang F, Gao F H, Yu J J. 2013. Geochronology and geochemistry of the Early Jurassic granitoids in the central Lesser Xing'an Range, NE China and its tectonic implications (in Chinese). Acta Petrol Sin, 29: 354–368

Xu P, Wu F Y, Xie L W, Yang Y H. 2004. Hf isotopic compositions of the standard zircons for U-Pb dating. Chin Sci Bull, 49: 1642–1648

Xu W L, Ji W Q, Pei F P, Meng E, Yu Y, Yang D B, Zhang X. 2009. Triassic volcanism in eastern Heilongjiang and Jilin Provinces, NE China: Chronology, geochemistry, and tectonic implications. J Asian Earth Sci, 34: 392–402

Xu W L, Pei F P, Wang F, Meng E, Ji W Q, Yang D B, Wang W. 2013. Spatial-temporal relationships of Mesozoic volcanic rocks in NE China: Constraints on tectonic overprinting and transformations between multiple tectonic regimes. J Asian Earth Sci, 74: 167–193

Yakubchuk A. 2002. The Baikalide-Altaid, Transbaikal-Mongolian and North Pacific orogenic collages: Similarity and diversity of structural patterns and metallogenic zoning. Geol Soc Lond Spec Publ, 204: 273–297

Yakubchuk A . 2004. Architecture and mineral deposit settings of the Altaid orogenic collage: A revised model. J Asian Earth Sci, 23: 761–779

Yang J H, Wu F Y, Shao J A, Wilde S A, Xie L W, Liu X M. 2006. Constraints on the timing of uplift of the Yanshan Fold and Thrust Belt, North China. Earth Planet Sci Lett, 246: 336–352

Yarmolyuk V V, Kovalenko V I, Salnikova E B, Budnikov S V, Kovach V P, Kotov A B, Ponomarchuk V A. 2002. Tectono-magmatic zoning, magma sources, and geodynamics of the Early Mesozoic Mongolia-Transbaikal Province. Geotectonics, 36: 293–311

Yu J J, Wang F, Xu W L, Gao F H, Pei F P. 2012. Early Jurassic mafic magmatism in the Lesser Xing'an-Zhangguangcai Range, NE China, and its tectonic implications: Constraints from zircon U-Pb chronology and geochemistry. Lithos, 142-143: 256–266

Zhang Q, Pan G Q, Li C D, Jin W J, Jia X Q. 2007. Does fractional crystallization occur in granitic magma? Some crucial questions on granite study (2) (in Chinese). Acta Petrol Sin, 23: 1239–1251

Zhao S, Xu W L, Tang J, Li Y, Guo P. 2016a. Timing of formation and tectonic nature of the purportedly Neoproterozoic Jiageda Formation of the Erguna Massif, NE China: Constraints from field geology and U-Pb geochronology of detrital and magmatic zircons. Precambrian Res, 281: 585–601

Zhao S, Xu W L, Tang J, Li Y, Guo P. 2016b. Neoproterozoic magmatic events and tectonic attribution of the Erguna Massif: Constraints from geochronological, geochemical and Hf isotopic data of intrusive rocks (in Chinese). Earth Sci, 41: 1803–1829

Zhao S, Xu W L, Wang F, Wang W, Tang J, Zhang Y H. 2016c. Neoproterozoic magmatisms in the Erguna massif, NE China: Evidence from zircon U-Pb geochronology (in Chinese). Geotectonica Metallogenia, 40: 559–573

Zhao S, Xu W L, Wang W, Tang J, Zhang Y H. 2014. Geochronology and geochemistry of Middle-Late Ordovician granites and gabbros in the Erguna region, NE China: Implications for the tectonic evolution of the Erguna Massif. J Earth Sci, 25: 841–853

Zhao Z H. 2016. Geochemical Principle of Trace Element (in Chinese). 2nd ed. Beijing: Science Press. 534

Zhao Z, Chi X G, Pan S Y, Liu J F, Sun W, Hu Z C. 2010. Zircon U-Pb LA-ICP-MS dating of Carboniferous volcanic and its geological significance in the Northwestern Lesser Xing'an Range (in Chinese). Acta Petrol Sin, 26: 2452–2464

Zhao Z. 2011. Late Paleozoic magmatism and its tectonic significance in the northern Great Xing'an Range, Northeastern China. Doctoral Dissertation (in Chinese). Changchun: Jilin University

Zhou C Y, Wu F Y, Ge W C, Sun D Y, Abbel R A A, Zhang J H, Cheng R Y. 2005. Age, geochemistry and petrogenesis of the cumulate gabbro in Tahe, northern Da Hinggan Mountain (in Chinese). Acta Petrol Sin, 21: 763–775